The Kinetics of Precipitate Dissolution in a Nickel-Base Superalloy

S.L. SEMIATIN, N.C. LEVKULICH, A.E. SAURBER, D.W. MAHAFFEY, E.J. PAYTON, and O.N. SENKOV

The effect of microstructure and soft impingement on the kinetics of static dissolution of γ' precipitates during supersolvus solution treatment of the powder-metallurgy nickel-base superalloy LSHR were determined experimentally and interpreted in the context of a simple diffusion model. The starting material had either a fine duplex structure of γ grains and γ' precipitates (each of which were ~2 μm in diameter) or a structure comprising ~2-μm-diameter γ' precipitates lying within large (~15 μm) γ grains. Using a direct-resistance-heated Gleeble® machine, the temperature of each sample was first equilibrated at a fixed subsolvus temperature (at which the microstructure was also stabilized) and then quickly raised to and held for a predetermined time in the single-phase γ field. The dissolution of γ' was found to be approximately five times as fast for the duplex structure in comparison to the kinetics for the intragranular precipitates. The results were interpreted using numerical simulations of dissolution based on the Whelan model modified to account for a distribution of precipitates (rather than a single, isolated spherical particle) and soft impingement of diffusion fields. Using independently-measured values for diffusivity, precipitate composition, and phase equilibria as input, simulation predictions showed good agreement with the observations in terms of the temporal variation of volume fraction and average particle radius. By this means, insight into the retarding influence of soft impingement and the accelerating effect of pipe diffusion (due to stored dislocations) on the rate of dissolution was obtained

DOI: 10.1007/s11661-017-4322-4

I. INTRODUCTION

THE dissolution of a precipitate phase plays an important role in the thermomechanical processing (TMP) of two-phase metallic alloys. Perhaps the most common application is age hardening. In such operations, coarse, second-phase particles are dissolved in a high-temperature single-phase field, the material is cooled quickly to retain a high supersaturation, and then it is aged at a moderate temperature in a two-phase field to develop a uniform distribution of precipitates with a substantially-refined size. Alloy systems that rely on age hardening include conventional aluminum-, iron-, beta-titanium-, and nickel- base alloys.

Fine-grain, powder-metallurgy (PM) nickel-base superalloys strengthened by the γ' phase comprise an alloy class for which an understanding of dissolution and subsequent precipitation is especially important. This is because γ' often serves a dual role as both a strengthening and a structure-control phase. With regard to the latter function, coarse, primary γ' (so-called because of its presence during hot working) pins γ boundaries and is thus instrumental in the development of fine, duplex microstructures during subsolvus processing. An excellent combination of strength and resistance to fatigue crack initiation are thereby obtained. By contrast, applications requiring service at which creep or creep-crack growth are life-limiting usually benefit from a coarse γ grain size produced by supersolvus solution treatment followed by controlled cooling. This operation sometimes leads to highly-undesirable abnormal grain growth (AGG) that can make a component unsuitable for service.[1]

Factors such as the strain rate imposed during subsolvus hot working[2–4] are thought to contribute to AGG during supersolvus heat-treatment of γ–γ' superalloys. In this respect, Soucail, Huron, and their coworkers[2,3] have demonstrated that subsolvus isothermal forging at strain rates near the transition from stage

S.L. SEMIATIN, D.W. MAHAFFEY, and E.J. PAYTON are with the Air Force Research Laboratory, Materials and Manufacturing Directorate, AFRL/RXCM, Wright-Patterson Air Force Base, OH 45433. Contact e-mail: sheldon.semiatin@us.af.mil N.C. LEVKULICH is with Wright-State University, Dayton, OH 45435. A.E. SAURBER is with the University of Dayton, Dayton, OH 45409. O.N. SENKOV is with UES, Inc., 4401 Dayton-Xenia Road, Dayton, OH 45432.

Manuscript submitted June 20, 2017.
Article published online September 25, 2017

II (superplastic) to stage III (power-law-creep) deformation are detrimental with regard to AGG during subsequent supersolvus heat treatment. In later work, the strain rate imposed during subsolvus forging was shown specifically to affect the location of γ' precipitates relative to the γ grain boundaries.[4,5] Thus, the rate of heating to and through the solvus, the manner in which intragranular *vs* grain-boundary γ' particles dissolve, and the release of the associated pinning forces may each play a significant role in AGG, as has been suggested in various investigations.[6–9]

During static, supersolvus heat treatment, the time required to dissolve γ' in PM superalloys is typically of the order of 1 to 4 minutes, the exact duration being a strong function of the temperature increment above the solvus.[10] The dissolution time can be shortened by approximately two orders of magnitude by concurrent deformation which leads to the formation of dislocation substructure/excess vacancies and thus significant pipe diffusion.[11] For example, γ' dissolution at and near the heated interface has been observed in inertia-friction welded samples for which the supersolvus temperature transient lasted only several seconds.[11,12] Moreover, an understanding of dissolution (and subsequent re-precipitation) kinetics is very important for the solid-state joining of *dissimilar* superalloys in which a graded precipitate microstructure developed in the heat-affected zone cannot be modified by a final heat treatment due to differences in solvus temperatures/approach curves of the two alloys.

Modeling and simulation of the kinetics of dissolution of γ' in nickel-base superalloys has received only moderate attention in the literature. Modeling techniques have comprised three principal categories: phenomenological, analytical, and phase-field. Perhaps the first attempt at developing a descriptive model was that due to Soucail and Bienvenu.[13] Assuming that the process is controlled by the diffusion of aluminum in nickel, they quantified the dissolution behavior for *continuous* heating cycles in terms of an effective time at the maximum exposure temperature and an effective diffusion distance for precipitates of various sizes. A complementary phenomenological approach (based on a JMAK-type analysis) was introduced by Cormier, Giraud *et al.*[14,15] to understand the effect of short-time heating transients on dissolution during the service of single-crystal superalloys. Giraud *et al.*[15] also showed that γ' dissolution is enhanced by relatively-small levels of strain introduced at γ–γ' interfaces during creep deformation.

The JMAK approach to describe the dissolution of an ensemble of γ' precipitates was subsequently utilized by Masoumi *et al.*[16] for the wrought superalloy AD730™. In addition, these authors briefly discussed the application of the analytical diffusion model of Whelan[17–19] to assess the effect of precipitate size on the dissolution time for an *isolated* particle in an infinite matrix. These latter results revealed the expected inverse dependence of dissolution time on the square of the particle radius first derived by Whelan.[17] The isolated-particle/infinite-matrix restriction was relaxed in the numerical (phase-field) simulations of Wang *et al.*,[20] in which the effect of a particle-size distribution (PSD) on dissolution behavior was investigated for the binary Ni-Al system. Here, it was shown that dissolution was predicted to be more rapid for the monosize-sphere case than for PSDs that were normal or log-normal. However, the specific simulation results were not validated experimentally.

The objective of the present work was to develop and validate a quantitative simulation method to predict the kinetics of γ' dissolution during static heat treatment of multi-component nickel-base superalloys. For this purpose, dissolution kinetics were measured for the superalloy LSHR with two different initial microstructural conditions: fine, duplex and coarse-γ-grain with intragranular precipitates. The measurements were interpreted using a numerical approach based on the Whelan analysis modified to treat the behavior of an arbitrary (initial) PSD and to incorporate the influence of overlapping diffusion fields (“soft impingement”).

II. MATERIAL AND EXPERIMENTAL PROCEDURES

A. *Material*

Because of the availability of carefully-measured phase-equilibria and diffusion data, the PM γ–γ' nickel-base superalloy LSHR was chosen to develop and apply a diffusion-based model for the dissolution of γ' precipitates during supersolvus heat treatment. LSHR (denoting “low-solvus, high refractory”) was developed by NASA for jet-engine-disk applications. It provides an attractive balance of properties at the bore and rim of disks that have been subjected to a graded-microstructure heat treatment in which only the component rim is exposed above the γ' solvus to promote local growth of fcc γ grains.[21,22]

The program material was identical to that used in several previous investigations of TMP, precipitation, and friction welding of PM superalloys.[4,5,12,23,24] It consisted of 230-mm-diameter extruded billet produced by Special Metals (Princeton, KY). Extrusion of such materials is typically done at a temperature of ~1339 K (1066 °C) and a reduction/ram speed that imparts an effective strain rate of ~1 s^{-1}. The material composition is given in Table I. In the as-received condition, the alloy had a fine, duplex microstructure of γ grains and *primary* γ' precipitates, each of whose average diameter was ~2 μm. There was also a small amount (<5 pct) of fine (≤400 nm) secondary (“cooling”) γ' and ~0.33 volume percent of carbide/boride particles with an average diameter of 315 nm. The γ'-solvus temperature, $T_{\gamma'}$, was 1430 K (1157 °C). The material showed a typical variation of γ' volume fraction with temperature (Figure 1).[24]

The material was used in two different microstructural conditions: the as-received, as-extruded condition (hereafter denoted as ARAE) and a second produced by an initial duplex solution treatment [1450 K (1177 °C) for 1 hour + furnace cool to 1311 K (1038 °C) + air cool] followed by a subsolvus γ' precipitate-coarsening treatment [1336 K (1093 °C) for 8 days + furnace cool to

Table I. Chemical Composition (Weight Percent) of LSHR Program Material

Co	Cr	Al	Ti	Mo	W	Nb	Ta	C	B	Zr	Ni
20.4	12.3	3.5	3.5	2.7	4.3	1.5	1.5	0.045	0.027	0.05	bal.

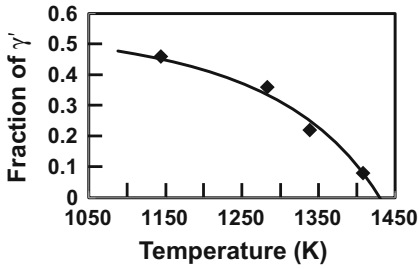

Fig. 1—Equilibrium γ' solvus-approach curve for LSHR. The data points are measurements; the solid line is an analytical fit to the data.[24]

1311 K (1038 °C) + air cool]. This treatment (referred to as SSHTPC) yielded an annealed microstructure of coarse γ grains (~14 μm in diameter) with intragranular γ' precipitates (~2 μm in diameter). As previously shown *via* grain-reference-orientation-deviation (GROD) measurements using electron backscatter diffraction (EBSD) and transmission electron microscopy observations on similar powder metallurgy superalloys,[6,25] the supersolvus portion of this heat treatment also eliminated the vast majority of the residual dislocation content associated with prior subsolvus hot working which had been pinned by the γ' precipitates.

B. *Experimental Procedures*

Short-time, isothermal experiments were performed using a direct-resistance-heated Gleeble® 3800-499 thermal-mechanical test system (manufactured by Dynamic Systems, Inc. (DSI) Poestenkill, NY) to establish the kinetics of γ' dissolution in LSHR and thereby obtain data needed for validation of diffusion-base models. To this end, cylindrical samples were extracted from the program material with the two-different starting microstructures *via* electrical-discharge machining followed by lathe turning to final dimensions of 6-mm diameter × 110-mm length.

Heat treatments in the Gleeble® machine utilized stainless steel (“hot”) jaws and low-force (“floating”) grips to minimize axial temperature gradients and to avoid the introduction of plastic strain due to thermal expansion during heating, respectively. The test temperature was controlled by a type-K thermocouple (made from chromel and alumel wire manufactured by Omega Engineering, Stamford CT) which was spot welded at the mid-length/outer-diameter (surface) location of each sample. Because of the very large dependence of the γ' dissolution rate on the precise increment of temperature above the solvus and the uncertainty associated with Type K thermocouples (±0.75 pct), preliminary work focused on calibration of the temperature at the cylinder-axis location (at which post-heat-treatment microstructures were characterized) against that indicated by surface thermocouples made from the same batch of wire. To this end, a series of isothermal, long-time, *near-subsolvus* heat treatments were performed, and the local temperatures at various radial locations within the sample were inferred from measurements of the γ' area fraction[26] and the solvus approach curve for LSHR.[24] By this means, it was determined that the temperature indicated by the surface (control) thermocouple was lower than that at the axis of the test sample by 30 ± 2K (30 ± 2 °C). This correction factor is therefore included in all experimental temperatures reported in the remainder of this paper.

Dissolution heat treatments comprised initial heating to 1339 K (1066 °C) and soaking for 15 minutes to equilibrate the temperature and microstructure. At this temperature, the equilibrium fraction of γ' in LSHR is 0.25 (Figure 1). (A comparison of metallographic observations of the volume fraction of γ' in samples quenched after 15 minutes at 1339 K (1066 °C) and that indicated on the solvus-approach curve confirmed that equilibrium had been reached.) Following the soak, the temperature was increased at a rate of 111 K/s (111 °C/s) to one of two supersolvus temperatures [1450 K or 1477 K (1177 °C or 1204 °C)], held at temperature for a time between 0 and 240 seconds, and then water quenched. Temperature overshoot during heating at the high rate was avoided by use of a slower heating ramp just before the peak temperature and adjustment of the PID controller per guidance from the equipment manufacturer. For experiments on the ARAE material at the higher supersolvus temperature, two separate dissolution campaigns were performed to obtain statistically significant data in view of the relatively short dissolution time in such instances.

Following heat treatment, each sample was sectioned transversely at the thermocouple location and prepared using standard metallographic techniques; *i.e.*, ground with SiC papers down to 800 grit, rough polished with diamond, and final polished with colloidal silica. The area fraction of γ' precipitates was determined *via* point counting on backscattered-electron (BSE) images. The images, covering multiple gamma grains, were taken at 1000X and 5000X magnifications at the cylinder-axis location using Sirion and Quanta scanning electron microscopes (SEMs) (FEI, Hillsboro, OR), each outfitted with a BSE detector manufactured by Deben U.K. Ltd. (London, U.K.); the accelerating voltage was 15 to 20 kV and the aperture size was 30 μm. At least 2 typical images (superimposed with ~3000 point-count grid intersections) were each “read” independently by three individuals for each heat treatment; with this approach, the confidence level was estimated to be >95 pct with scatter in the volume-fraction measurements of approximately ±0.005 or less.

The number of precipitates per unit area was also determined manually for each heat-treatment condition.

From the precipitate area fraction and number-density results, the average two-dimensional (2D) circle-equivalent diameter (CED) was determined; the scatter in this quantity was ±0.05 μm. For selected conditions, the 2D CED PSD was estimated *via* measurement of the diameter of at least 100 discrete precipitate particles. In addition, EBSD was used to estimate the average γ grain size in the ARAE and SSHTPC samples. EBSD data were obtained using an XL-30 SEM (FEI, Hillsboro, OR) with EDAX/TSL OIM^{TM} software (EDAX Corp., Mahwah, NJ). The step size was 0.1 to 0.4 or 1 μm for the ARAE and SSHTPC samples, respectively. For the ARAE samples, data cleanup was utilized to remove features whose number of pixels was comparable to or smaller than the area of typically-smaller (incoherent) γ' precipitates in samples that had undergone substantial dissolution.

To facilitate the interpretation of precipitate observations and the numerical simulation of dissolution, the approximate correspondence between the average 3D diameter of a distribution of spherical particles and that observed in 2D sections was determined using MATLAB®. For this purpose, a number of hypothetical distributions of spherical particles, each with a specified volume fraction and standard deviation, were instantiated into a cubic box. For each instantiation, a number of arbitrarily-oriented sections through the box were taken, and the average diameter of the 2D circular sections through the particles determined and compared to the average 3D diameter.

III. RESULTS

The direct-resistance-heating method was successful in providing well-controlled heating cycles characterized by a rapid rise time, no overshoot, prescribed soak time at the dissolution temperature, and rapid cooling *via* water quenching at the end of the thermal cycle (*e.g.*, Figure 2). In Figure 2, the small delay at the end of the hold at the high temperature (~0.2 seconds) corresponded to the time interval between that at which the power was shut off and the quench began. Post-heat-treatment results consisted of (1) microstructural observations and (2) quantitative characterization of the microstructures in terms of the γ' precipitate fraction, average size, and size distribution and the γ grain size.

A. *Microstructure Observations*

Backscattered-electron (BSE) images revealed the effect of initial (preform) microstructure, supersolvus solution temperature, and time on γ' dissolution. In the BSE images, γ' is the darker particulate phase; the fine, white particles are borides/carbides which are not soluble at the temperatures of interest here.

The dissolution behavior was readily imaged for the samples whose initial structure comprised coarse γ' within large γ grains that had been produced *via* supersolvus heat treatment followed by a long-time, subsolvus coarsening treatment, *i.e.*, the SSHTPC condition. High- and low-magnification images (Figures 3, 4, respectively) for such samples heat treated at 1450 K (1177 °C), *i.e.*, 20 K (20 °C) above the equilibrium solvus temperature, showed an initial rapid decrease in the fraction of γ', followed by a drop-off in rate at long times of the order of 120 seconds. After the longest time used (240 seconds), there were still a few remnant γ' precipitates. As will be discussed later, this behavior is as expected in view of the decrease with time of the matrix supersaturation*, which supplies the driving force for dissolution.

*During the dissolution of a second phase in a multi-component system, the matrix may be supersaturated or depleted in solute depending on the equilibrium partitioning of the specific solute between the matrix and precipitate. As discussed below, γ' dissolution in γ–γ' superalloys is controlled by the diffusion of chromium which is *supersaturated* in the matrix. Thus, in this work, the term supersaturation is used to connote the non-equilibrium concentration of rate-limiting solute in the matrix during the dissolution process.

Similar qualitative trends were noted for samples with the as-received, as-extruded (ARAE) preform microstructure that were also heat treated at 1450 K (1177 °C) (Figures 5, 6). The most noticeable difference was the shorter time scale over which dissolution occurred. Specifically, the majority of the γ' precipitates had dissolved by 30 seconds. The elimination of the γ' and its associated grain-boundary pinning effect was also evidenced by a marked increase in γ grain size between 10 and 30 seconds, a trend that persisted to longer times as well. Nevertheless, a few scattered γ' precipitates were evident at 60 seconds and longer times.

A sharp dependence of dissolution rate on temperature was deduced by a comparison of the microstructures developed in ARAE samples heat treated at 1450 K (1177 °C) (Figures 5, 6) *vs* 1477 K (1204 °C) (Figure 7). At the higher heat-treatment temperature, a substantial reduction in γ' fraction and increase in γ grain size was observed after only 10 seconds, corresponding to an approximately fourfold increase in kinetics compared to the lower supersolvus temperature.

B. *Quantitative Microstructure Characterization*

The broad trends described in the previous section were substantiated by quantitative measurements of the fraction and average size of the γ' precipitates (Figure 8). For both preform microstructures and supersolvus dissolution temperatures, the fraction of γ' decreased exponentially with time (Figure 8(a)). A comparison of the time to reduce the fraction of γ' from the initial value of 0.25 to a specified level (*e.g.*, 0.05) revealed that dissolution at the fixed temperature of 1450 K (1177 °C) was approximately five times faster for the ARAE microstructure as for the SSHTPC structure despite having comparable initial (average) γ' diameters. Similarly, a fourfold increase in kinetics for the ARAE microstructure when the temperature was raised from 1450 K to 1477 K (1177 °C to 1204 °C) was borne out by the measurements for a γ' fraction of ~0.02 (Figure 8(a)).

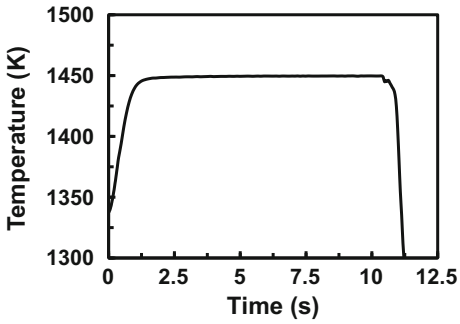

Fig. 2—Typical temperature-*vs*-time profile for an LSHR sample that was rapidly heated from 1339 K (1066 °C), soaked 10 s at 1450 K (1177 °C), and then water quenched.

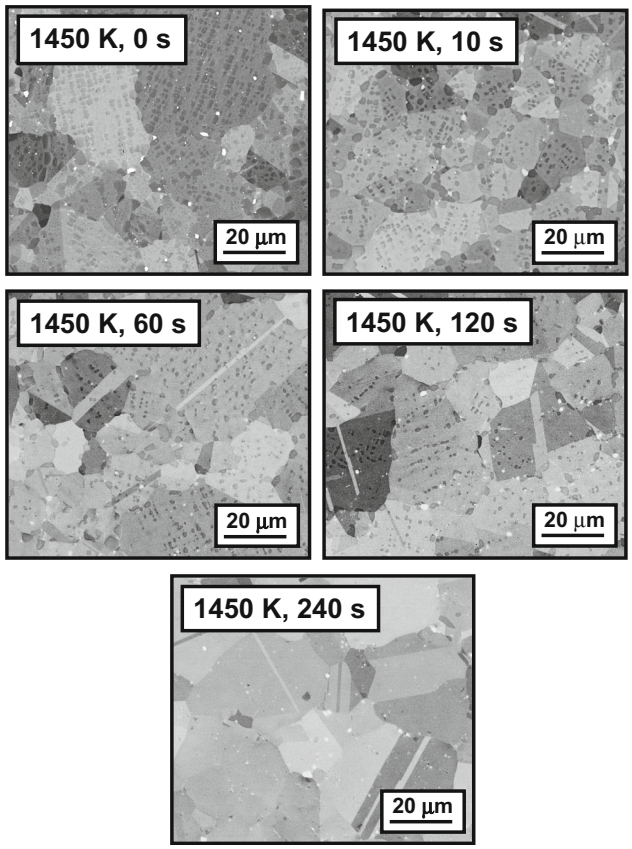

Fig. 3—Low-magnification BSE images of LSHR samples with the SSHTPC preform microstructure that were subjected to an isothermal dissolution treatment at 1450 K (1177 °C) for the times indicated.

Measurements of the temporal variation in average 2D precipitate size (Figure 8(b)) did not show a continuous decrease with increasing time. For the SSHTPC microstructure, for example, it appeared that the average diameter decreased rapidly for times of the order of 0 to 60 seconds and then remained fairly constant. This observation is analogous to that noted by Payton *et al.*[10] Its source can be rationalized on the basis of the rapid dissolution of the finest precipitates at short

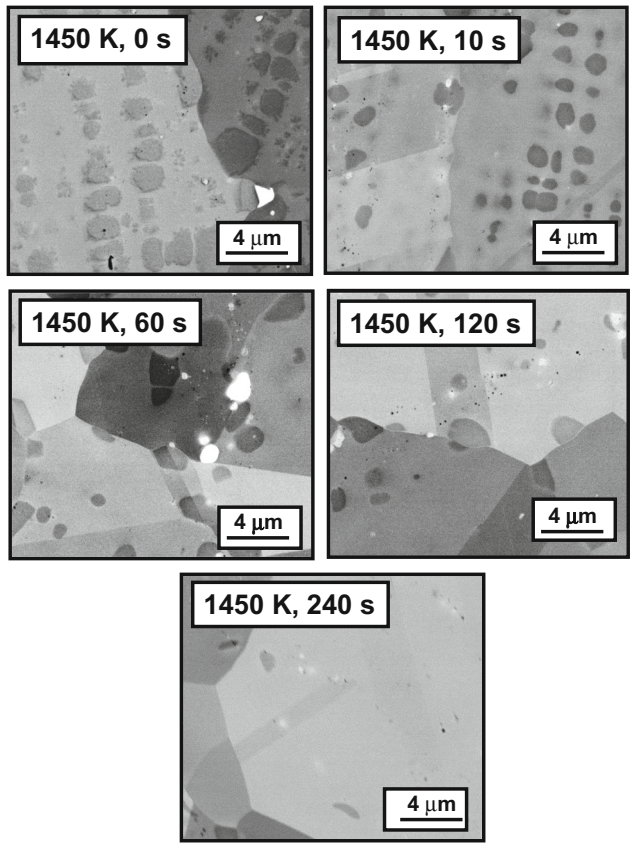

Fig. 4—High-magnification BSE images of LSHR samples with the SSHTPC preform microstructure that were subjected to an isothermal dissolution treatment at 1450 K (1177 °C) for the times indicated.

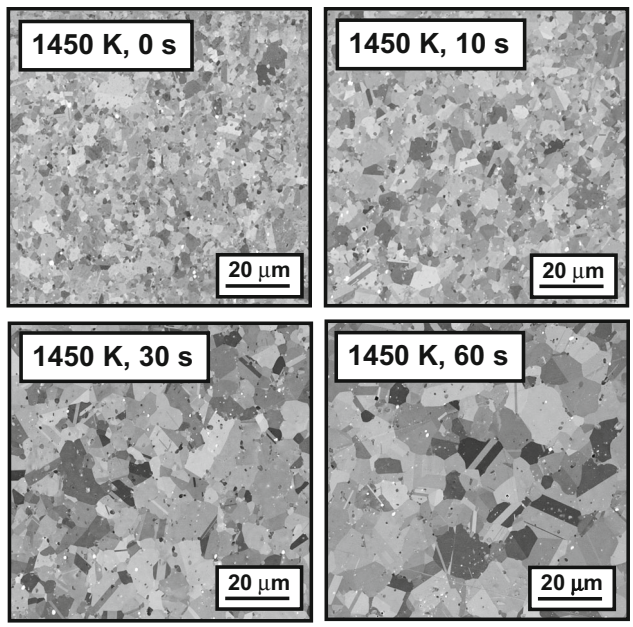

Fig. 5—Low-magnification BSE images of LSHR samples with the ARAE preform microstructure that were subjected to an isothermal dissolution treatment at 1450 K (1177 °C) for the times indicated.

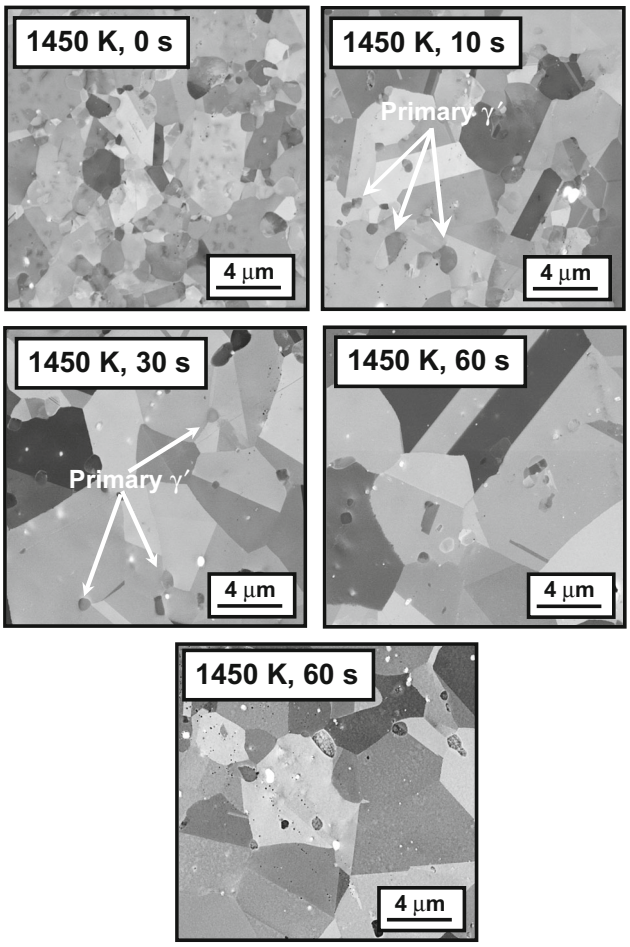

Fig. 6—High-magnification BSE images of LSHR samples with the ARAE preform microstructure that were subjected to an isothermal dissolution treatment at 1450 K (1177 °C) for the times indicated.

times (*i.e.*, when the supersaturation is very high) followed by slower dissolution of the remaining precipitates into a matrix of decreased supersaturation.

The time dependence of the average γ' size for the experiments with the ARAE material, for which initial 2D diameter was ~1.6 μm, also suggested a rapid initial decrease in average size followed by an approximately steady-state regime (Figure 8(b)).

The ARAE data for the fraction of γ' as a function of time (Figure 8(a)) were mirrored by corresponding EBSD measurements of the evolution of the γ grain size (Figure 9). At 1450 K (1177 °C), for example, the γ grain size exhibited a marked increase for times between ~30 to 90 seconds. This time interval was similar to that over which the majority of the γ' dissolved and thus the associated pinning force was eliminated. Similarly, an abrupt change in γ grain size was observed at 1477 K (1204 °C) for times between ~10 and 30 seconds. These times also coincided with the period during which most of the γ' dissolved. Grain-size data at longer times suggested the attainment of a near steady state for which the remnant pinning force was provided by insoluble borides and carbides.

Selected measurements of the 2D γ' particle size distribution (PSD) showed lognormal-like behavior. This was evidenced in the histograms of frequency *vs* particle size (*e.g.*, Figures 10(a) and (b)) and corresponding probability plots (Figure 10(c)). With regard to the latter, the behavior was nearly linear except for "tails" at the low and high ends. As discussed by Semiatin *et al.*,[23] the low-end tail is likely an artifact of 2D sectioning which is weighted by sectioned particles, thus masking their true 3D size. Furthermore, the results in Figure 10(c) suggested that the maximum particle diameter was approximately twice the average diameter, a finding in line with classical work on the evolution of precipitate PSDs during static coarsening.[27]

IV. DISCUSSION

The LSHR γ'-dissolution measurements were interpreted in the context of the classical Whelan model[17] modified to account for evolving supersaturation and a distribution of precipitate sizes. By this means, the effects of overlapping concentration fields and stored work introduced prior to dissolution on kinetics were quantified. As pointed out by Aaron and Kotler,[18,19] however, stationary-interface approaches such as that of Whelan are strictly applicable to small supersaturations, which pertain to the *latter* stages of dissolution in the present work, but not to the initial behavior. For large supersaturations, Whelan[17] and Gang *et al.*[20] have suggested that the rate of dissolution is *less* than that predicted by the model. Hence, the following predictions should be considered as a *lower* bound for the dissolution time. Despite this drawback, the Whelan model did provide a framework for investigating the broad influence of material parameters on kinetic behavior.

A. *Modified Whelan Model*

The Whelan model[17] pertains to the dissolution of an isolated spherical precipitate of radius R in an infinite matrix, for which the following simple differential equation was derived:

$$\frac{dR}{dt} = -\frac{kD}{2R} - \frac{k}{2}\sqrt{\frac{D}{\pi t}}, \qquad [1]$$

In Eq. [1], t denotes time, D is the diffusivity, and k is the matrix supersaturation defined as the following:

$$k = \frac{2(C_I - C_M)}{(C_P - C_I)}. \qquad [2]$$

Here, C_I, C_M, and C_P represent the compositions of the matrix at the matrix-precipitate interface, the matrix far from the interface, and the precipitate at the interface, respectively. For a diffusion-controlled reaction, it is assumed that C_I and C_P correspond to the equilibrium matrix composition immediately adjacent to the particle and the particle composition, respectively.[17–19] The first and second terms on the right-hand

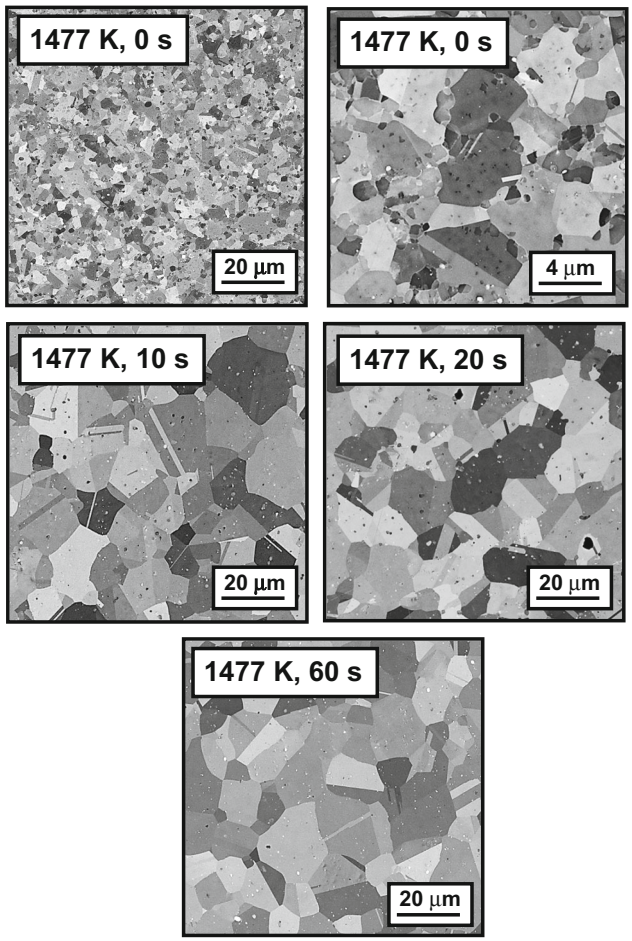

Fig. 7—BSE images of LSHR samples with the ARAE preform microstructure that were subjected to an isothermal dissolution treatment at 1477 K (1204 °C) for the times indicated.

side of Eq. [1] come from the steady-state and transient parts of the diffusion field, respectively.

The effect of soft impingement on the 'far-field' matrix composition C_M was taken into account in the present work using the typical approximation derived from a mass balance[28]:

$$C_M = \frac{(C_o - f_{\gamma'} C_{\gamma'})}{(1 - f_{\gamma'})}, \quad [3]$$

in which C_o and $f_{\gamma'}$ denote the overall alloy composition and the volume fraction of the precipitate (γ') phase. The composition of γ' was assumed to be constant and thus taken to be equal to C_P.

To relax the isolated-particle assumption in the Whelan model, an initial log-normal particle-size distribution (Figure 11) was assumed per the experimental observations in Section III. The distribution had a standard deviation of 0.3 times the normalized mean and was divided into 10^5 bins with evenly-spaced radii R_i ($i = 1,2,\ldots 10^5$) for numerical simulations. Although characterized in terms of its initial *number fraction* of precipitates, each bin also had a specific initial *volume fraction* ($f_{\gamma,io}$) associated with it such that the total initial volume fraction of precipitates was equal to that developed at the subsolvus temperature used to equilibrate the initial microstructure in the experiments, *i.e.*, 0.25.

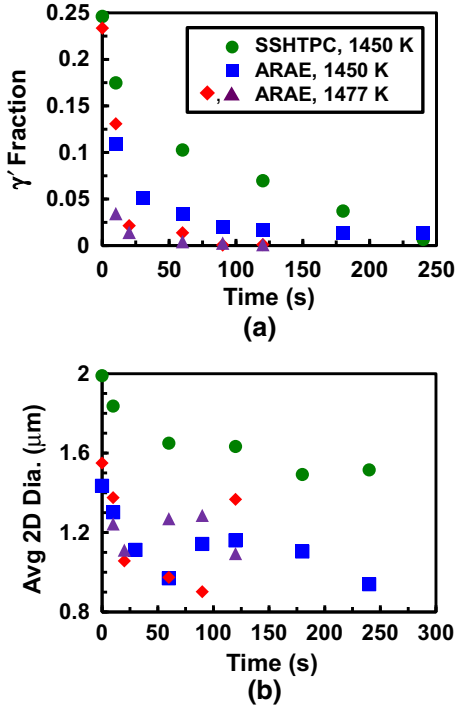

Fig. 8—Measurements of (*a*) γ' fraction and (*b*) the average 2D (circle-equivalent) diameter of the γ' precipitates as a function of time for LSHR samples with the two different preform microstructures that were subjected to an isothermal dissolution treatment.

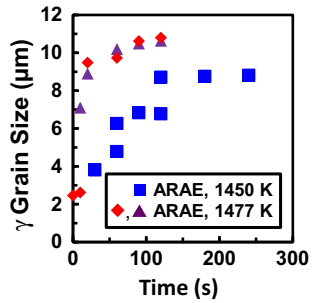

Fig. 9—Average gamma grain size as function of time during dissolution heat treatment of ARAE samples at 1450 K (1177 °C) (blue data points) or 1477 K (1204 °C) (red, purple data points) (Color figure online).

Numerical simulations were performed using a computer code written in Python™. For a given simulation, the initial far-field matrix composition (C_M, Eq. [3]) and equilibrium composition of the matrix at the matrix-precipitate (C_I) for the specific dissolution temperature were first calculated. Assumed to be the same for all precipitate sizes, the initial supersaturation was then calculated using Eq. [2], and an increment of dissolution was applied for the precipitates within each bin per Eq. [1]. The volume fraction of the precipitate in each bin was then updated per its new radius, *viz.*,

$$f_{\gamma' i} = f_{\gamma' i_o} \left(R_{i/} R_{i_o} \right)^3, \quad [4]$$

and the total volume fraction $f_{\gamma'}$ and matrix composition C_M (Eq. [3]) were also updated. Another increment of dissolution was then applied in a similar manner. Once the size of the precipitates within a given bin reached zero, its contribution to the distribution was eliminated.

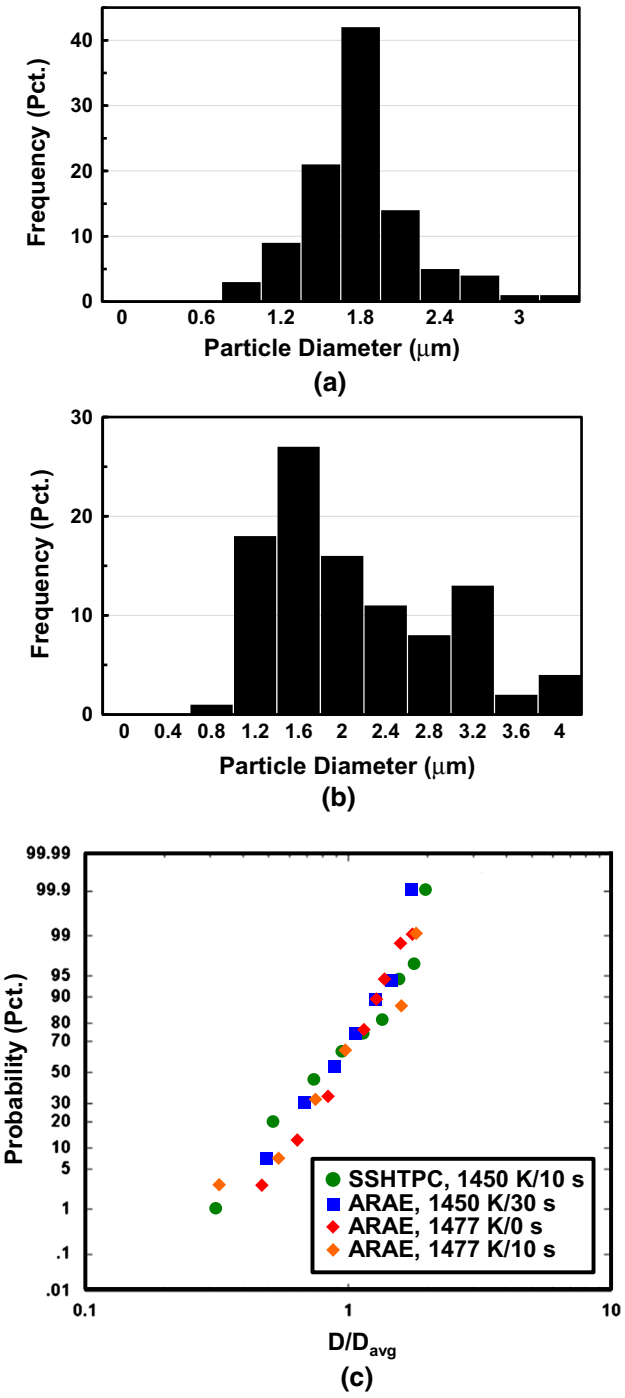

Fig. 10—Precipitate-size-distribution measurements: (*a*, *b*) Typical 2D circle-equivalent-diameter (CED) results and (*c*) cumulative probability plot for 2D CED.

B. *Input Data for Simulations*

In addition to the initial PSD, the input data required for the simulations comprised values of D and C_I pertinent to the specific dissolution temperature.

To avoid possible errors and uncertainties in kinetic databases for multi-component PM superalloys such as LSHR, an effective diffusivity (D_{eff}) determined previously (and independent of the present dissolution trials) for an annealed (nominally strain-free) matrix was utilized. Specifically, former work demonstrated that chromium is the rate-limiting solute for processes such as nucleation, growth, and coarsening of γ' in LSHR and similar materials.[24,29,30] Furthermore, it was shown that predictions of the coarsening rate constant from a Lifshitz-Slyosov-Wagner (LSW) model modified for a finite volume fraction of precipitates showed good agreement with measurements for temperatures between 1116 K and 1366 K (843 °C and 1093 °C) when using an effective diffusivity between 0.25 and 0.4 times the diffusivity of chromium in nickel (D_{Cr}). The same values of diffusivity were then shown to produce excellent agreement between measured and predicted values of the average size and number per unit volume of secondary γ' precipitates produced during cooling following a supersolvus annealing treatment. Hence, the following diffusivity was used in the present work on dissolution of γ':

$$\begin{aligned} D\ (\mu m^2/s) &= D_{eff} = 0.33 \times D_{Cr} \\ &= 1.188 \times 10^8 \exp(-34280/T(K)). \end{aligned} \quad [5]$$

At 1450 K and 1477 K (1177 °C and 1204 °C), D_{eff} was equal to 6.39×10^{-3} or 9.97×10^{-3} $\mu m^2/s$, respectively. Thus, the diffusivity was only ~50 pct greater at the higher temperature relative to that at the lower temperature.

The value of the matrix composition C_I in equilibrium with the precipitate was estimated from the assumed-constant precipitate composition and the equilibrium solvus approach curve ($f_{\gamma'}$ *vs* T). Assuming that dissolution behavior is controlled by chromium diffusion, as above, the atomic fraction of Cr in the precipitate (taken to be constant) is 0.0211.[24,29] The corresponding matrix composition was determined from a mass-balance equation in conjunction with the overall

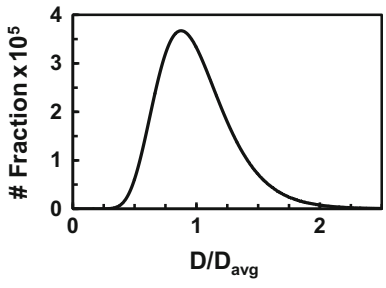

Fig. 11—Precipitate-size distribution in terms of number fraction *vs* normalized diameter used in dissolution simulations with 100,000 bins.

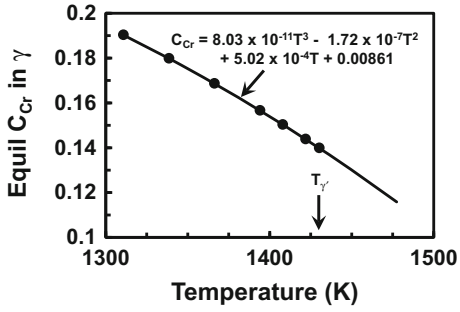

Fig. 12—Chromium content (atomic fraction) in γ phase in equilibrium with γ' precipitate as a function of absolute temperature.

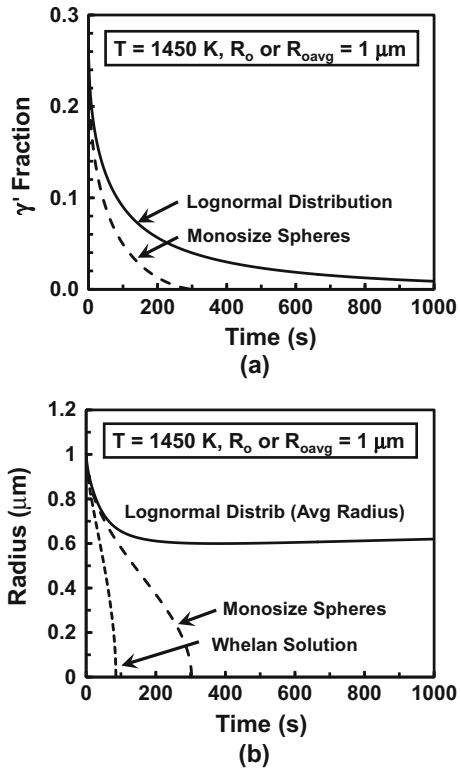

Fig. 13—Simulation predictions of the dissolution of γ' at 1450 K (1177 °C) as a function of time assuming a starting particle radius/average radius of 1 μm: (*a*) γ' fraction and (*b*) radius/average radius.

alloy chromium content (0.14 atomic fraction) and an analytical fit to $f_{\gamma'}$ *vs* T (Figure 1),[24,29] *i.e.*,

$$C_{Cr} = (0.14 - 0.0211\ f_{\gamma'})/(1 - f_{\gamma'}) \quad [6]$$

$$\text{in which} \quad f_{\gamma'} = -\frac{4C^*\left(1 - \exp\left[\frac{Q}{R}\left(\frac{T-T_{\gamma'}}{T\cdot T_{\gamma'}}\right)\right]\right)}{1 - 4C^*\exp\left[\frac{Q}{R}\left(\frac{T-T_{\gamma'}}{T\cdot T_{\gamma'}}\right)\right]} \quad [7]$$

Here, C* denotes the atomic fraction of gamma-prime formers in the alloy (~0.535 for LSHR), and Q is a fitting parameter (= 60 kJ/mol). The subsolvus dependence of C_{Cr} on temperature so obtained was fit to a third-order polynomial, which was then extrapolated to

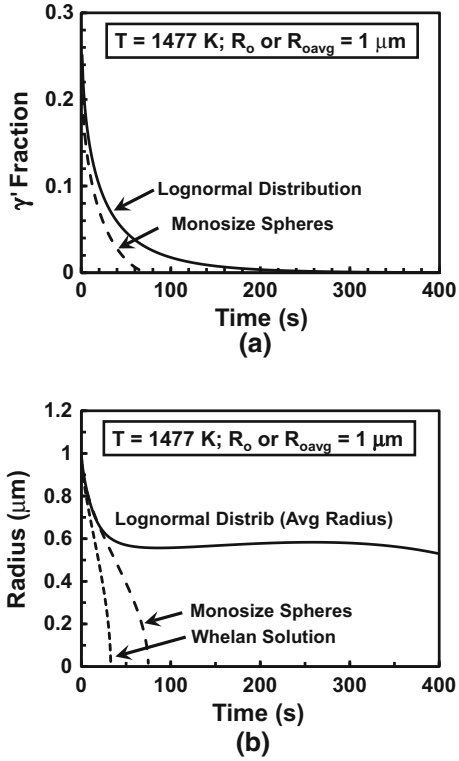

Fig. 14—Simulation predictions of the dissolution of γ' at 1477 K (1204 °C) as a function of time assuming a starting particle radius/average radius of 1 μm: (*a*) γ' fraction and (*b*) radius/average radius.

the supersolvus dissolution temperatures used in the present work (Figure 12).

C. *Simulation Predictions*

1. *Initial simulations*

Initial simulation predictions for *spherical* precipitates with a starting diameter/average diameter of 2 μm (radius = 1 μm) illustrated the effects of precipitate size distribution, soft impingement, and temperature on dissolution kinetics. Three cases were examined: (i) a distribution of monosize precipitates (denoted as MSP) with an initial volume fraction of 0.25, (ii) a lognormal size distribution (denoted as LNSD) of precipitates (per Figure 11) with an initial volume fraction of 0.25, and (iii) an isolated precipitate in an infinite matrix (*i.e.*, the Whelan solution). For cases (i) and (ii), soft impingement was treated as described in Section IV–A. Dissolution behavior was quantified in terms of predictions of volume fraction and average precipitate radius as a function of time for each of two temperatures, 1450 K and 1477 K (1177 °C and 1204 °C) (Figures 13 and 14, respectively).

At 1450 K (1177 °C), the predicted variation of γ' fraction with time exhibited a very rapid decrease at short times ($t \le 60$ seconds) for both the MSP and LNSD simulations (Figure 13(a)). At longer times, the former case showed more rapid dissolution. In particular, the time to reach a γ' fraction of 0.01 was ~200 seconds for MSP and ~500 seconds for the LNSD. The source of the difference can be ascribed to the fact

that all of the precipitates in the MSP case experienced the same instantaneous supersaturation and thus shrank at the same rate, whereas the last-to-disappear (initially-largest) precipitates in the LNSD case dissolved into a matrix with a much-depleted supersaturation.

The retardation of dissolution due to soft impingement and an initial particle-size distribution was quantified further in simulation results for size/average size (Figure 13(b)). The LNSD simulation showed a nominally-constant precipitate size after an initial sharp decrease during which the smallest precipitates had dissolved (*i.e.*, for $0 < t \leq 60$ seconds). The fact that the finer precipitates dissolved first, thereby leaving larger ones, would have retarded kinetics in view of the inverse dependence of dissolution rate on R at long times (Eq. [1]) and the reduced supersaturation. The effect of reduced supersaturation (due to soft impingement) on dissolution behavior is further illustrated in Figure 13(b) through a comparison of MSP and LNSD behaviors with predictions from the Whelan solution. For the Whelan case, the supersaturation was assumed to retain its initial (high) value, and thus the predicted dissolution rate was much more rapid than that predicted for the MSP and LNSD cases, *i.e.*, by a factor of ~3 or ~10, respectively.

The simulation trends for 1477 K (1204 °C) (Figure 14) were qualitatively similar to those for the lower temperature except that the kinetics were enhanced by a factor of ~4 for the MSD and LNSD cases and a factor of ~2 for the Whelan solution. The difference in enhancement was largely due to the impact of higher supersaturation at the higher temperature and its major influence on dissolution behavior.

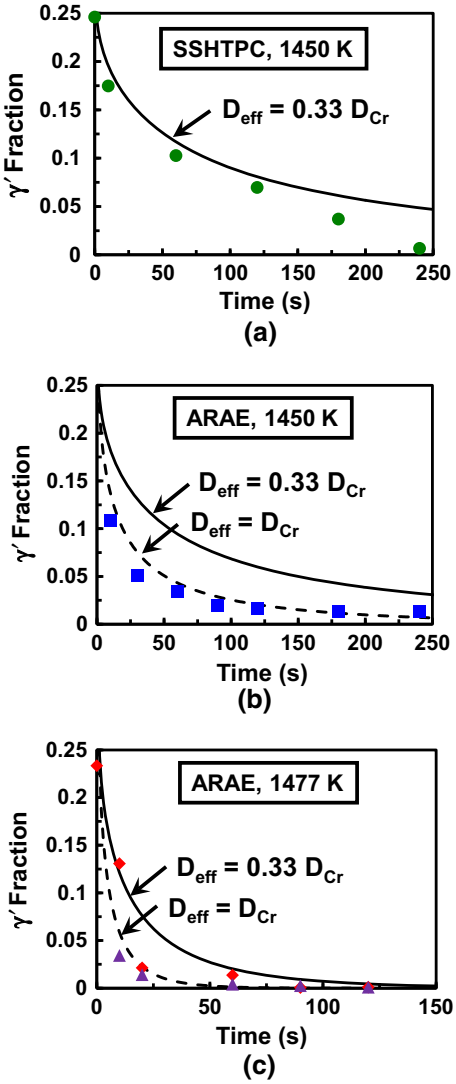

Fig. 15—Comparison of measurements (data points) and predictions (lines) of the γ' fraction as a function of time for (*a*) SSHTPC samples at 1450 K (1177 °C), (*b*) ARAE samples at 1450 K (1177 °C), and (*c*) ARAE samples at 1477 K (1204 °C). In (b, c), the measured values are compared to simulation predictions for two different values of D_{eff}.

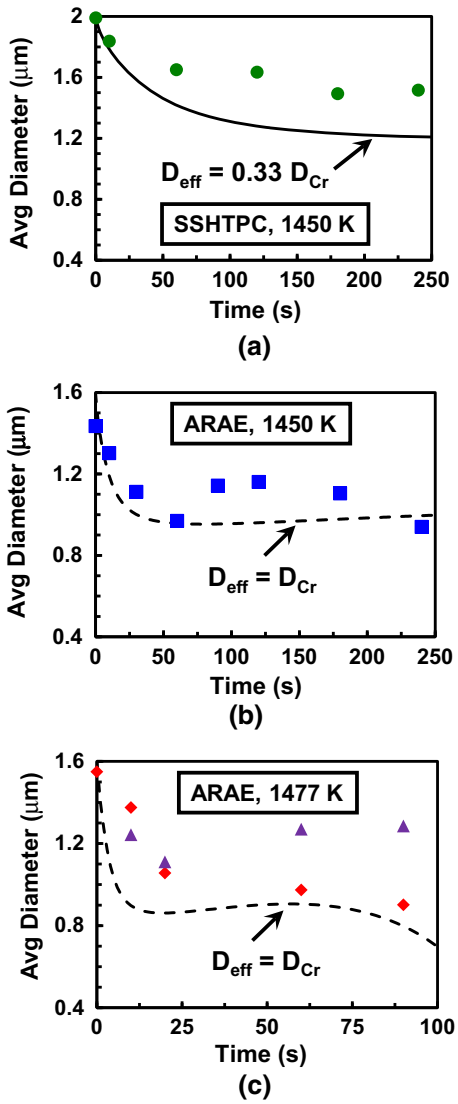

Fig. 16—Comparison of measurements (data points) and predictions (lines) of average precipitate diameter as a function of time for (*a*) SSHTPC samples at 1450 K (1177 °C), (*b*) ARAE samples at 1450 K (1177 °C), and (*c*) ARAE samples at 1477 K (1204 °C).

2. *Comparison of measured and predicted dissolution behaviors*

Simulations which treated the effect of soft impingement on the concentration field and an initial lognormal precipitate-size distribution yielded predictions of the temporal evolution of the γ' fraction and average precipitate diameter which showed reasonably good agreement with the measurements for LSHR summarized in Section III.

Taking $D_{eff} = 0.33 \times D_{Cr}$, the predicted variation of γ' fraction with time for SSHTPC samples at 1450 K (1177 °C) showed good agreement with measurements for $t \leq 100$ seconds (Figure 15(a)). At longer times, simulation predictions started to diverge from the observations. This difference could be due to a slightly non-uniform initial distribution of precipitates experimentally which could have affected the evolution of supersaturation around larger remnant particles, especially at long times. The greater-than-predicted dissolution rate for long times suggested that the supersaturation had been *higher* than average for the final particles to dissolve. Further research to investigate this hypothesis (using a method such as phase-field analysis) is warranted.

For ARAE samples, simulations using $D_{eff} = 0.33 \times D_{Cr}$ broadly *underestimated* the rate of dissolution at both heat-treatment temperatures (Figures 15(b) and (c)). On the other hand, it was found that the observations at both temperatures were well fit by additional simulations for which the effective diffusivity was *three* times as large, *i.e.*, $D_{eff} = D_{Cr}$. From a mechanistic standpoint, the required higher effective diffusivity can be rationalized on the basis of enhanced (pipe) diffusion arising from dislocation substructure remaining from the extrusion operation used to make the as-received program material. As suggested by Payton[6] and DeMania,[25] such substructure would have been pinned by γ' precipitates until they dissolved. The magnitude of the apparent enhancement of diffusion suggested by the comparison of measured and predicted dissolution behaviors in the present work (*i.e.*, three-fold) can be compared to previous efforts in the literature. For example, Masoumi *et al.*[11] have suggested that *concurrent* deformation can enhance the high-temperature diffusivity of substitutional solutes in nickel-base superalloys by a factor of ~25. On the other hand, the experimental work of Weiss and Jonas[31] for HSLA steels showed that the enhancement of diffusion by hot working *prior to* heat treatment is approximately one-tenth that when the deformation is *concurrent* with the diffusional process. In the present work, the fact that dislocation substructure is also annealed out as the γ' precipitates dissolve above the solvus suggests that the approximate three-fold enhancement of diffusion (as suggested by the comparison of simulation and experimental results in Figures 15(b) and (c)) is thus not unreasonable.

The absence of noticeable substructure (and perhaps the coarser γ grain size) in SSHTPC samples, whose initial synthesis comprised a supersolvus annealing treatment, can thus be concluded to be the source of observed much slower dissolution behavior in comparison to the ARAE samples.

Simulation predictions of the average size of the γ' precipitates (using the corresponding values of D_{eff} which provided the best fit for the γ'-fraction results) showed approximate agreement with the measurements (Figure 16). For these comparisons, a stereological factor was *not* introduced to adjust the 2D circle-equivalent diameter measurements despite the 3D-nature of the simulation predictions. This approach was justified in light of MATLAB® simulations (described in Section II–B) which showed that the so-called correction factor can approach unity for lognormal size distributions whose maximum particle size is approximately 2.5 times the average; such a trend was also described by Louis and Gokhale.[32] With this proviso, the plots in Figure 16 indicated that the precipitate-size predictions mirrored the measurements at least qualitatively. The tendency for the measurements to lie *above* the simulation predictions can be rationalized on the basis of the fact that the measurements likely overlooked some of the very fine precipitates (*e.g.*, those whose diameter was ≤0.2 μm), whose neglect would have had a small effect on the measured γ' fraction but which would have led to an *overestimate* of the average size.

V. SUMMARY AND CONCLUSIONS

The static dissolution of γ' precipitates during the supersolvus heat treatment of LSHR samples in two different starting conditions was measured and interpreted in the context of a series of diffusion simulations. From this work, the following conclusions have been drawn:

1. For a given starting average precipitate size, dissolution kinetics are considerably slower for a microstructure comprising γ' precipitates within large γ grains (produced by prior supersolvus heat treatment and extended subsolvus coarsening) in comparison to that developed by subsolvus extrusion. The enhanced dissolution rate for the latter microstructure is likely due to pipe diffusion associated with retained substructure.
2. Despite the stationary-interface assumption used to derive the Whelan solution for the dissolution of an isolated, spherical precipitate in an infinite matrix, reasonable quantitative estimates of the kinetics of dissolution of an aggregate of γ' particles during supersolvus heat treatment can be obtained by the numerical integration of the pertinent differential equation provided account is taken of soft impingement of adjacent diffusion fields and the evolution of the average matrix composition and associated supersaturation.
3. The enhanced rate of dissolution of γ' with relatively-small increases in temperature above the solvus is due to concurrent increases in the solute diffusivity and supersaturation.
4. An effective diffusivity, which is a specific fraction of the diffusivity of chromium in binary Ni-Cr alloys, can be used to model dissolution kinetics to a first order.

ACKNOWLEDGMENTS

This work was conducted as part of the in-house research of the Metals Branch of the Air Force Research Laboratory's Materials and Manufacturing Directorate. The yeoman assistance of P.N. Fagin, J.O. Brown, and Z.A. Partlow in conducting the experiments is gratefully acknowledged. Three of the authors were supported under the auspices of Contracts FA8650-14-2-5800 (NCL, AES) and FA8650-15-D-5230 (ONS).

REFERENCES

1. J.W. Martin, R.D. Doherty, and B. Cantor: *Stability of Microstructure in Metallic Systems*, Cambridge University Press, Cambridge, UK, 1997.
2. M. Soucail, M. Marty, and H. Ocor: in *Superalloys 1996*, R.D. Kissinger, D.J. Deye, D.L. Anton, A.D. Cetel, M.V. Nathal, T.M. Pollock, and D.A. Woodford, eds., TMS, Warrendale, PA,1996, pp. 663–66.
3. E. Huron, S. Shrivatsa, and E. Raymond: in *Superalloys 2000*, T.M. Pollock, R.D. Kissinger, R.R. Bowman, K.A. Green, M. McLean, S. Olson, and J.J. Schirra, eds., TMS, Warrendale, PA, 2000, pp. 49–58.
4. S.L. Semiatin, K.E. McClary, A.D. Rollett, C.G. Roberts, E.J. Payton, F. Zhang, and T.P. Gabb: *Metall. Mater. Trans. A*, 2013, vol. 44A, pp. 2778–98.
5. S.L. Semiatin, J.M. Shank, A.R. Shiveley, W.M. Saurber, E.F. Gaussa, and A.L. Pilchak: *Metall. Mater. Trans. A*, 2014, vol. 45A, pp. 6231–51.
6. E.J. Payton: Ph.D. Dissertation, The Ohio State University, Columbus, OH, 2009.
7. P.R. Rios: *Acta Mater.*, 1997, vol. 45, pp. 1785–89.
8. K. Song and M. Aindow: in *Proc. Materials Science and Technology (MS&T) 2006: Fundamentals and Characterization, Vol. 2*, Z-K. Lu, C.E. Campbell, L.Q. Chen, E. B. Damm, J.E. Morral, and J.L. Murray, eds., TMS, Warrendale, PA, 2006, pp. 211–220.
9. G. Wang, D.S. Xu, E.J. Payton, N. Ma, R. Yang, M.J. Mills, and Y. Wang: *Acta Mater.*, 2011, vol. 59, pp. 4587–94.
10. E.J. Payton, T.A. Wynn, and M.J. Mills: *J. Mater. Sci.*, 2012, vol. 20, pp. 7305–11.
11. F. Masoumi, D. Shahriari, M. Jahazi, J. Cormier, and B.C.D. Flipo: *Metall. Mater. Trans. A*, 2017, vol. 48A, pp. 2886–99.
12. O.N. Senkov, D.W. Mahaffey, S.L. Semiatin, and C. Woodward: *Metall. Mater. Trans. A*, 2014, vol. 45A, pp. 5545–61.
13. M. Soucail and Y. Bienvenu: *Mater. Sci. Eng. A*, 1996, vol. A220, pp. 215–22.
14. J. Cormier, X. Milhet, and J. Mendez: *J. Mater. Sci.*, 2007, vol. 42, pp. 7780–86.
15. R. Giraud, Z. Hervier, J. Cormier, G. Saint-Martin, F. Hamon, X. Milhet, and J. Mendez: *Metall. Mater. Trans. A*, 2013, vol. 44A, pp. 131–46.
16. F. Masoumi, M. Jahazi, D. Shahriari, and J. Cormier: *J. Alloy. Compd.*, 2016, vol. 658, pp. 981–95.
17. M.J. Whelan: *Metal Sci. J.*, 1969, vol. 3, pp. 95–97.
18. H.B. Aaron and G.R. Kotler: *Metall. Trans.*, 1971, vol. 2, pp. 393–408.
19. H.B. Aaron and G.R. Kotler: *Metal Sci. J.*, 1970, vol. 4, pp. 222–25.
20. G. Wang, D.S. Xu, N. Ma, N. Zhou, E.J. Payton, R. Yang, M.J. Mills, and Y. Wang: *Acta Mater.*, 2009, vol. 57, pp. 316–25.
21. J. Gayda, T.P. Gabb, and P.T. Kantzos: in *Superalloys 2004*, K.A. Green, T.M. Pollock, H. Harada, T.E. Howson, R.C. Reed, J.J. Schirra, and S. Walston, eds., TMS, Warrendale, PA, 2004, pp. 323–30.
22. J. Lemsky: Report NASA/CR-2005-213574, Ladish Company, Inc., Cudahy, WI, February 2005 (available electronically at http://gltrs.grc.nasa.gov).
23. S.L. Semiatin, K.E. McClary, A.D. Rollett, C.G. Roberts, E.J. Payton, F. Zhang, and T.P. Gabb: *Metall. Mater. Trans. A*, 2012, vol. 43A, pp. 1649–61.
24. S.L. Semiatin, S.-L. Kim, F. Zhang, and J.S. Tiley: *Metall. Mater. Trans. A*, 2015, vol. 46A, pp. 1715–30.
25. D.E. DeMania: PhD Dissertation, University of Virginia, Charlottesvile, VA, 2002.
26. S.L. Semiatin, D.W. Mahaffey, N.C. Levkulich, and O.N. Senkov: *Metall. Mater. Trans. A*, 2017, DOI:10.1007/s11661-017-4296-2.
27. P.W. Voorhees and M.E. Glicksman: *Acta Metall.*, 1984, vol. 32, pp. 2013–30.
28. O. Grong and H.R. Shercliff: *Prog. Mater. Sci.*, 2002, vol. 47, pp. 163–282.
29. S.L. Semiatin, F. Zhang, R. Larsen, L.A. Chapman, and D.U. Furrer: *Integr. Mater. Manufact. Innov.*, 2016, vol. 5 (3), pp. 1–20.
30. T.P. Gabb, J. Gayda, D.F. Johnson, R.A. McKay,, R.B. Rogers, C.K. Sudbrack, A. Garg, I.E. Locci, S.L. Semiatin, and E. Kang: Report NASA/TM-2016-218936, NASA Glenn Research Center, Cleveland, OH, February 2016 (available electronically at http://gltrs.grc.nasa.gov).
31. I. Weiss and J.J. Jonas: *Metall. Trans. A*, 1979, vol. 10A, pp. 831–40.
32. P. Louis and A. Gokhale: *Metall. Mater. Trans. A*, 1995, vol. 26A, pp. 1741–44.